Realisation of broadband two-dimensional nonreciprocal acoustics using an active acoustic metasurface

Joe Tan,[1] Jordan Cheer,[1] and Charlie House[2]

[1] *Institute of Sound and Vibration Research, University of Southampton, Southampton, SO17 1BJ, United Kingdom*

[2] *Visiting Researcher at Institute of Sound and Vibration Research, University of Southampton, Southampton, SO17 1BJ, United Kingdom*[a]

(Dated: 3 September 2024)

Nonreciprocal acoustic devices have been shown to be able to control incident waves propagating in one direction, whilst allowing incident waves propagating in the opposite direction to be transmitted without modification. Nonreciprocal sound transmission has typically been achieved by introducing nonlinearities or directional biasing through fluid motion or spatiotemporal modulation of resonant cavities. However, the spatial arrangement of these approaches creates preferential characteristics in one direction, such that the direction of the nonreciprocal behaviour is fixed and, thus, they are not straightforwardly reconfigurable. To address this issue, it has previously been shown that feedforward wave-based active controllers can be used to drive a single subwavelength active unit cell to achieve broadband nonreciprocal sound transmission or absorption in a one-dimensional linear acoustic system. Extending this concept, this paper investigates how the feedforward wave-based active controller can be used to drive an array of subwavelength active unit cells forming a metasurface to achieve broadband nonreciprocal sound absorption over a two-dimensional plane. Through both simulation and experimental studies, this paper shows that active wave-based absorption control systems can achieve broadband nonreciprocal sound absorption when the incident waves are generated by both normally and obliquely-positioned primary sources.

[a] j.cheer@soton.ac.uk

I. INTRODUCTION

Reciprocity is an acoustic property that describes the symmetry in sound transmission between two points. For example, the acoustic response between an acoustic source and sensor is equal to the response when the acoustic source and sensor locations are swapped. Although a variety of acoustic applications have exploited reciprocity to simplify measurement processes[1,2], it is undesirable in certain applications. For example, nonreciprocal acoustic control could be exploited variously to improve privacy, to acoustically cloak objects or to enable improved sensing or manipulation of a sound field. This has led to significant interest in the development of nonreciprocal acoustic devices that achieve one-way sound transmission. Previously proposed nonreciprocal acoustic devices have generally broken the symmetry in transmission by introducing nonlinearities[3–7], fluid motion[8] or spatiotemporal modulation of resonant cavities[9–11]. These various approaches have different limitations: nonlinear nonreciprocal acoustic devices typically require high input power and are often bulky; additional unwanted noise is introduced when fluid motion is introduced; resonant cavities can only achieve nonreciprocal behaviour over a narrow bandwidth and finally, all of these nonreciprocal devices are not straightforwardly tuneable to reverse the direction of the nonreciprocal behaviour. The majority of these limitations have been addressed through the development of non-local active metamaterials that contain non-collocated sensor and actuator pairs[12,13]. However, the spatial arrangement of the sensor and actuator pairs still creates preferential characteristics in one direction and, thus, the direction of the nonreciprocal behaviour is still fixed in this case. More recently, the issue of tuneability has been addressed through the development of feedforward wave-based active control systems that drive one subwavelength active unit cell to minimise the transmitted and reflected wave components individually to achieve broadband nonreciprocal sound transmission or absorption in a one-dimensional linear acoustic system[16]. This wave-based active controller achieves broadband nonreciprocal control by taking advantage of the causality of feedforward control. By setting the positive propagating incident wave as the reference signal, this controller minimises the corresponding wave components with respect to the positive propagating incident wave, whilst the negative propagating incident wave propagates unimpeded since the reference signal to the controller in this case is near-zero and the wave-based active controller only controls the wave components that are associated with the reference signal. The advantage of a wave-based active control system is that it is fully tuneable, such that the direction of the nonreciprocal behaviour can be easily reversed by changing the reference and error signals in the feedforward controller.

Since the study of nonreciprocal acoustic devices is a fairly new topic, there has been limited investigation into how nonreciprocal behaviour can be achieved in two or three-dimensional spaces[17,18]. Building on the wave-based active control concept, this paper therefore presents an investigation into how the feedforward wave-based active controller proposed in[16] can be extended to form a metasurface, consisting of an array of control sources and arrays of pressure sensors, which is used to minimise the transmitted and reflected wave components to achieve broadband nonreciprocal sound absorption in a two-dimensional plane within a three-dimensional space. This extension over the work presented in[16] not only includes extension to a multi-input, multi-output metasurface, but also includes the introduction of a more complex wave-separation technique that is able to handle primary wave fields with spherical wave fronts and non-normal angles of incidence. Therefore, this paper presents two main research contributions: firstly, it is demonstrated how the wave-based active controller can be extended to drive an active metasurface to achieve nonreciprocal sound absorption across a two-dimensional plane and secondly, it is shown that the wave separation method can handle spherical wave fronts and obliquely-positioned primary sources. The performance of the proposed wave-based actively controlled metasurface has initially been investigated via simulations using an analytical free field model with monopole acoustic sources. The proposed methodology is then investigated using the responses measured for a practical system constructed in the anechoic chamber at the Institute of Sound and Vibration Research (ISVR).

II. SYSTEM DESCRIPTION

The physical arrangement of the proposed wave-based nonreciprocal actively controlled metasurface is shown in Figure 1. The system consists of a dual-layer array of monopole control sources, which are indicated by the crosses in Figure 1, and dual-layer arrays of pressure sensors positioned either side of the control source array. The dual layer array of sources is required to be able control the reflected and transmitted wave components; whilst the dual layer arrays of sensors are required to be able to sense the incident, reflected and transmitted wave components variously. The incident acoustic fields propagating in the positive and negative directions are generated by primary sources located either side of the control source and sensor arrays, as also shown in Figure 1. The acoustic field can be described in terms of wave components, which are indicated by the coefficients A to D in Figure 1. It is worth noting that the coefficients A to D represent different wave components depending on the direction of the incident sound field. When the incident sound field is generated by a positive primary source, A and C are the positive propagating incident and transmitted waves respectively and B and D are the negative propagating upstream and downstream reflected wave components respectively. Conversely, when the incident sound field is produced by a negative primary source, D and B are the negative propagating incident and transmitted waves respectively and C and A are the positive propagating upstream and downstream reflected wave components respectively. The subscripts $_+$ and $_-$ are used throughout this paper to distinguish whether a wave component is generated by a positive or negative primary source. Each pressure sensor in Figure 1 is denoted by the following notation: the first subscript indicates the sensor plane within which the sensor is located and the second subscript indicates which of the L-th pressure sensors within that sensor plane is being referred to. L is also the number of error signals, which will be described in Section IV.

The geometric parameters that define the system shown in Figure 1 are presented in Table I. The frequency range of interest for this investigation has been defined between 150 Hz and 400 Hz. The lower limit is based on the low frequency performance of the loudspeakers used to practically realise the control sources in the experimental implementation and the upper frequency limit has been chosen to avoid spatial aliasing by ensuring that the spacing between control sources and sensors in the y-direction is less than half the shortest acoustic wavelength. The frequency range could be extended by using loudspeakers with an improved low frequency performance and reducing the spacing in the y-direction between adjacent sources and pressure sensors. However, these requirements are somewhat contradictory, since improving the low frequency performance of loudspeakers typically requires their size to increase which in turn will limit how close to each other the loudspeakers can be placed.

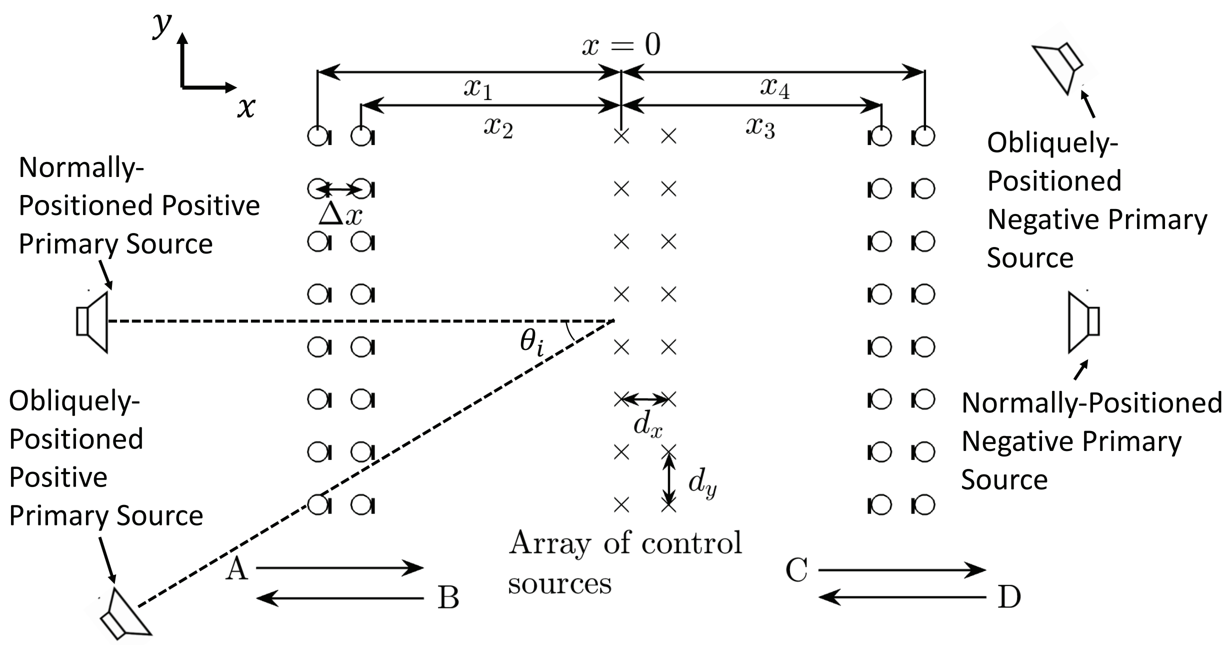

FIG. 1. The system geometry used to realise nonreciprocal sound absorption in a two-dimensional plane via the wave-based actively controlled metasurface. The black crosses indicate the locations of control sources and the circles denote the locations of the pressure sensors. The primary sources are denoted by loudspeaker diagrams, but their positions in the subsequent investigations are not shown to scale in this diagram.

It is important to note that we have assumed in this paper that we are considering control of the sound field in a two-dimensional plane within a three-dimensional space. This means that we are able to control the sound field using line arrays of sources and sensors, as shown

Variable	Value	Variable	Value
d_y	0.4 m	d_x	0.11 m
Δx	0.15 m	x_1	-0.725 m
x_2	-0.575 m	x_3	0.615 m
x_4	0.765 m		

TABLE I. The parameters used to define the system shown in Figure 1.

in Figure 1, rather than the grids of sources and sensors that would be required to control over three-dimensional space. The methodology described here could be extended to control over a full three-dimensional space, but in addition to grids of sources and sensors, would also require an extension of the wave separation method described in the next section to use a two-dimensional Spatial Fourier Transform. This is left for future work, mainly due to the practical challenge of realising such a large experimental implementation.

III. WAVE SEPARATION METHOD

The wave separation method described in this section focuses primarily on the case when the incident wave is generated by a positive primary source, as shown in Figure 1, however, the same methodology can also be used in the case of a negative primary source. As in[16], the positive propagating incident, A_+, transmitted, C_+, and reflected, B_+, wave components need to be separated from the total pressure measured at each pressure sensor in the system shown in Figure 1 because they are used as the reference and error signals in the case of controlling a positive primary source. This separation of wave components has been carried out using a wave separation method based on the Spatial Fourier Transform (SFT). The advantages of this approach are that no assumptions are made regarding the nature of the sound field and it is straightforward to apply to the linear arrays utilised here[19–22]. In addition, the SFT has the ability to decompose the pressure distribution of spherical waves into their plane wave components. For the system shown in Figure 1, a one-dimensional SFT is required to transform the spatial y-coordinate to the wavenumber domain variable k_y, which can be written as

$$p(x, k_y) = \int_{-\infty}^{\infty} p(x, y)\mathrm{e}^{-\mathrm{j}k_y y} dy \tag{1}$$

where

$$k_y = k_0 \sin\theta, \tag{2}$$

k_y is the component of the wavenumber in the y-direction and θ is the angle of incidence. Practically, it is not straightforward to apply the SFT given by Eq. 1 due to the integral of the pressure over an infinite space, however, it has previously been shown that this can be approximated by the sum of the weighted pressures at several sampling points[22]. Thus, the transformed sound pressure at the l-th pressure sensor in the p-th pressure sensor plane, whose positions are indicated by the variables x_1 to x_4 shown in Figure 1, can be expressed as[22]

$$p_{p_l}(x_{p_l}, y_{p_l})W(y_{p_l}) \tag{3}$$

where

$$W(y_{p_l}) = \mathrm{e}^{-\mathrm{j}k_y y_{p_l}}, \tag{4}$$

subscript $_p$ denotes the sensor plane, $W(y_{p_l})$ is the weighting factor that applies the appropriate phase shift corresponding to the angle between the location of the lth pressure sensor and the plane perpendicular to the incident wave direction, k_0. When the incident angle is zero, the pressure sensor planes are already perpendicular to the incident wave direction and, thus, the weighting factors given by Eq. 4 are equal to unity. For time domain implementation, the ideal impulse responses of the weighting factors can be obtained via inverse Fourier transform of Eq. 4, however, the impulse responses in this case are non-casual, which limits their application within a control system. Causality can, however, be maintained by incorporating modelling delays into the weighting factor responses, which was previously proposed in[23]. This allows the delayed weighting factors to be modelled using Finite Impulse Response (FIR) filters, which have been designed in this case using a least mean squares fitting approach[24].

Using the delayed and weighted pressure measured at each pressure sensor according to Eq. 3, the same wave separation method described in[25] can then be used to calculate the positive and negative propagating waves at each pair of closely spaced pressure sensors in the upstream and downstream spaces. In this wave separation method, the total pressure, p_l, and particle velocity, u_l, at the midpoint of the l-th pair of closely spaced pressure sensors in the upstream section is calculated as

$$p_l = \frac{p_{1_l} W(y_{1_l}) + p_{2_l} W(y_{2_l})}{2}, \tag{5}$$

and

$$u_l = \frac{1}{\rho_0 \Delta x} \int_0^{T_s} p_{1_l} W(y_{1_l}) - p_{2_l} W(y_{2_l}) \; dt, \tag{6}$$

where p_{1_l} and p_{2_l} are the pressures measured by the sensors at the l-th position in the first and second sensor planes, T_s is the sampling period and ρ_0 is the density of air. The positive and negative propagating waves at the l-th pair of closely spaced pressure sensors can be calculated as

$$A_l = \frac{1}{2}\Big(p_l + \rho_0 c_0 u_l\Big), \tag{7}$$

and

$$B_l = \frac{1}{2}\Big(p_l - \rho_0 c_0 u_l\Big), \tag{8}$$

where c_0 is the speed of sound in air. Substituting Eqs. 5 and 6 into Eqs. 7 and 8, the positive and negative propagating waves at the lth pair of closely spaced pressure sensors can also be expressed as

$$\begin{aligned} A_l = &\frac{p_{1_l} W(y_{1_l}) + p_{2_l} W(y_{2_l})}{4} \dots \\ &+ \frac{c_0}{2\Delta x} \int_0^{T_s} p_{1_l} W(y_{1_l}) - p_{2_l} W(y_{2_l})\ dt, \end{aligned} \tag{9}$$

and

$$\begin{aligned} B_l = &\frac{p_{1_l} W(y_{1_l}) + p_{2_l} W(y_{2_l})}{4} \dots \\ &- \frac{c_0}{2\Delta x} \int_0^{T_s} p_{1_l} W(y_{1_l}) - p_{2_l} W(y_{2_l})\ dt. \end{aligned} \tag{10}$$

The wave separation method described in this section has also been applied to the third and fourth planes of pressure sensors to calculate the wave components, C_l and D_l, at the l-th pair of pressure sensors in the downstream space and the transmitted wave component at the l-th pair of closely spaced pressure sensors can be calculated as

$$\begin{aligned} C_l = &\frac{p_{3_l} W(y_{3_l}) + p_{4_l} W(y_{4_l})}{4} \dots \\ &+ \frac{c_0}{2\Delta x} \int_0^{T_s} p_{3_l} W(y_{3_l}) - p_{4_l} W(y_{4_l})\ dt, \end{aligned} \tag{11}$$

where p_{3_l} and p_{4_l} are the pressures measured by the sensors at the l-th position in the third and fourth sensor planes.

IV. WAVE-BASED ACTIVE CONTROL FORMULATION

Once the transmitted and reflected wave components have been separated from the total pressure measured at each pair of pressure sensors using the wave separation method described in Section III, these wave components can be used to realise control. The proposed wave-based active control system uses a multichannel feedforward Filtered-Reference Least Mean Squares (FxLMS) algorithm to adaptively control the corresponding wave components and the block diagram for this active control system is shown in Figure 2. The FxLMS algorithm is the most widely utilised adaptive feedforward control strategy for active noise control and its implementation and operation has been widely discussed[26]. The vector of $2L$ error signals is generated by combining the L reflected, B_{+l}, and L transmitted, C_{+l}, wave components, whilst the positive propagating incident wave, A_{+_l}, for the L pairs of pressure sensors are used to generate the vector of L reference signals. As mentioned in Section I, the advantage of the proposed wave-based actively controlled metasurface is that the direction of the nonreciprocal behaviour can be straightforwardly reversed by changing the reference and error signals used by the wave-based controller shown in Figure 2, however, this is not demonstrated explicitly here for conciseness.

In the considered configuration, the dual layer array of control sources are driven to minimise the transmitted, C_{+_l}, and reflected, B_{+_l}, wave components with respect to the incident acoustic field generated by the positive primary source, whilst allowing the incident

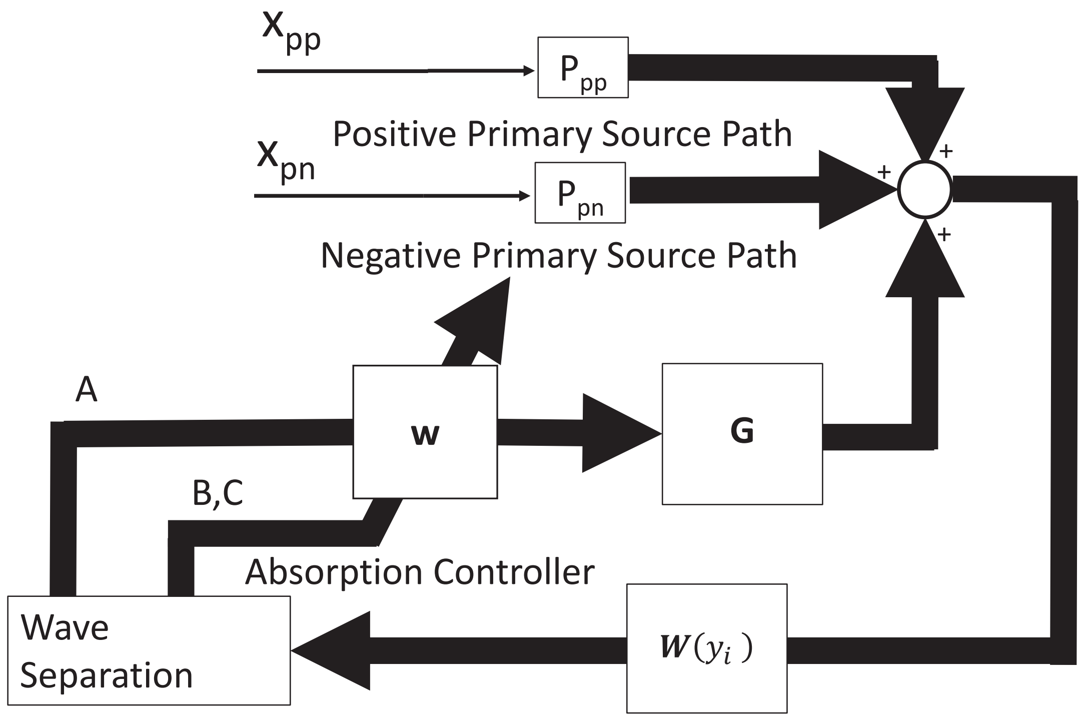

FIG. 2. The block diagram of the wave-based active controller used to drive the dual-layer array of control sources forming the metasurface to achieve nonreciprocal sound absorption.

acoustic field generated by the negative primary source to propagate freely, thus achieving nonreciprocal sound absorption. The vector of error signals in this case can be defined at the n-th time sample as

$$\mathbf{e}(n) = \mathbf{d}(n) + \mathbf{R}(n)\mathbf{w}(n) \tag{12}$$

where

$$\mathbf{e}(n) = \begin{bmatrix} e_{T_1}(n) & e_{R_1}(n) & \ldots & e_{T_L}(n) & e_{R_L}(n) \end{bmatrix}^T, \tag{13}$$

is the vector of $2L$ error signals;

$$\mathbf{d}(n) = \begin{bmatrix} d_{T_1}(n) & d_{R_1}(n) & \ldots & d_{T_L}(n) & d_{R_L}(n) \end{bmatrix}^T, \tag{14}$$

is the vector of $2L$ disturbance signals comprised of the transmitted and reflected wave components generated by the positive primary source, where the l-th reflected and transmitted wave components are given by Eqs. 10 and 11 respectively;

$$\mathbf{w}(n) = \begin{bmatrix} w_{11_i}(n), & w_{12_i}(n), & \dots & w_{MKI}(n) \end{bmatrix}^T \tag{15}$$

is the $2MKI$ vector of FIR control filter coefficients, where M is the number of control sources, K is the number of reference signals, which is equal to L in this case and I is the length of each FIR control filter;

$$\mathbf{R}(n) = \begin{bmatrix} \mathbf{r}_{T_1}(n) & \mathbf{r}_{T_1}(n-1) & \dots & \mathbf{r}_{T_1}(n-I-1) \\ \mathbf{r}_{R_1}(n) & \mathbf{r}_{R_1}(n-1) & \dots & \mathbf{r}_{R_1}(n-I-1) \\ \mathbf{r}_{T_2}(n) & \mathbf{r}_{T_2}(n-1) & \dots & \mathbf{r}_{T_2}(n-I-1) \\ \mathbf{r}_{R_2}(n) & \mathbf{r}_{R_2}(n-1) & \dots & \mathbf{r}_{R_2}(n-I-1) \\ \vdots & \vdots & \ddots & \vdots \\ \mathbf{r}_{T_L}(n) & \mathbf{r}_{T_L}(n-1) & \dots & \mathbf{r}_{T_L}(n-I-1) \\ \mathbf{r}_{R_L}(n) & \mathbf{r}_{R_L}(n-1) & \dots & \mathbf{r}_{R_L}(n-I-1) \end{bmatrix}, \tag{16}$$

is the $(2L \times MKI)$ matrix of transmitted and reflected wave components calculated from the filtered reference signals, where the l-th vector of reflected, $\mathbf{r}_{R_l}(n)$, and transmitted, $\mathbf{r}_{T_l}(n)$, wave components have been defined as

$$\mathbf{r}_{R_l}(n) = \begin{bmatrix} r_{R_{l11}}(n) & r_{R_{l12}}(n) & \dots & r_{R_{lMK}}(n) \end{bmatrix}^T, \tag{17}$$

and

$$\mathbf{r}_{T_l}(n) = \begin{bmatrix} r_{T_{l11}}(n) & r_{T_{l12}}(n) & \dots & r_{T_{lMK}}(n) \end{bmatrix}^T, \tag{18}$$

where $r_{R_{lmk}}(n)$ and $r_{T_{lmk}}(n)$ are the reflected and transmitted wave components calculated from the filtered reference signals according to Eqs. 10 and 11 respectively. The reference signals have been filtered by the FIR filter that represents the plant response between the m-th control source and l-th pressure sensor within the p-th sensor plane, which have been calculated based on an initial identification phase as standard in FxLMS implementations. These filtered reference signals are given by

$$r_{p_{lm}} = \sum_{j=0}^{J-1} g_{p_{lmj}} A_{+_l}(n-j), \tag{19}$$

where A_{+_l} is the l-th reference signal corresponding to the incident wave component and g_{plmj} is the j-th FIR filter coefficient of the J coefficient filter representing the plant response between the m-th control source and the l-th pressure sensor within the p-th plane of pressure sensors. The cost function in this case is the sum of the mean squared error signals, which can be expressed as

$$J(n) = \mathbb{E}\left[\mathbf{e}^T(n)\mathbf{e}(n)\right]. \tag{20}$$

Substituting Eq. 12 into Eq. 20, the cost function can be expressed in Hermitian quadratic form as

$$\begin{aligned} J(n) = \mathbf{w}^T(n)\mathbf{R}^T(n)\mathbf{R}(n)\mathbf{w}(n)... \\ +2\mathbf{w}^T(n)\mathbf{R}^T(n)\mathbf{d}(n) + \mathbf{d}^T(n)\mathbf{d}(n). \end{aligned} \tag{21}$$

Taking the derivative of the cost function with respect to the vector of FIR control filter coefficients, the resulting gradient can be expressed as

$$\begin{aligned} \frac{\partial J(n)}{\partial \mathbf{w}(n)} &= 2[\mathbf{R}^T(n)\mathbf{R}(n)\mathbf{w}(n) + \mathbf{R}^T(n)\mathbf{d}(n)]... \\ &= 2\mathbf{R}(n)\mathbf{e}(n). \end{aligned} \tag{22}$$

Using the negative gradient given by Eq. 22, the multichannel FxLMS algorithm can be used to adapt the vector of FIR control filter coefficients to minimise the transmitted and reflected wave components as

$$\mathbf{w}(n+1) = \mathbf{w}(n) - \mu\mathbf{R}(n)\mathbf{e}(n), \tag{23}$$

where μ is the convergence gain, which controls the speed and stability of the adaptation.

V. SIMULATION STUDY

In order to investigate the performance of the proposed actively controlled metasurface under ideal conditions, this section presents the results from a simulation based investigation, where the control sources and primary sources are modelled as monopoles in a free field environment and the sensors are assumed to be omnidirectional. The performance of the proposed wave-based active controller described in Section IV is evaluated when it is subject to an incident sound field that is generated by either normally or obliquely-positioned positive or negative primary sources. The performance of the proposed controller is evaluated using the magnitude of the pressure transmission and reflection coefficients averaged across the array of L , which is defined for a positive incident primary source as

$$T = \frac{1}{L}\sum_{l=1}^{L}\left|\frac{C_{+l}}{A_{+l}}\right|, \tag{24}$$

$$R = \frac{1}{L}\sum_{l=1}^{L}\left|\frac{B_{+l}}{A_{+l}}\right| \tag{25}$$

and the power absorption coefficient defined using the averaged pressure transmission and reflection coefficients as

$$\alpha = 1 - (|T|^2 + |R|^2). \tag{26}$$

Despite the fact that the system shown in Figure 1 only considers a two-dimensional plane, the incident sound field produced by both primary sources has been assumed to radiate spherically into three dimensional space, in order to be consistent with the experimental configuration described in Section II. As a result, the incident sound field and performance metrics in the uncontrolled case encounter losses due to spherical spreading. To ensure consistency between the theoretical and experimental results, the theoretically-modelled acoustic responses between each acoustic source and each pressure sensor have been modelled as outgoing spherical waves, which can be expressed as

$$p(r) = \frac{p_0}{|r|} e^{-\mathrm{j}k_0|r|} \tag{27}$$

where r is the distance between the acoustic source and the pressure sensor, p_0 is the pressure amplitude and $|.|$ is an Euclidean norm. The losses due to spherical spreading are included in these simulated acoustic responses via the $\frac{1}{|r|}$ term in Eq. 27. To demonstrate nonreciprocal behaviour, the performance metrics in the controlled and uncontrolled cases are compared for both positive and negative incident primary fields, in the case of normal or obliquely positioned primary sources, and these results are presented in the following subsections.

A. Normally-Positioned Primary Source

In the first instance, the performance metrics have been calculated before and after implementing the proposed wave-based active controller when the fields incident on the metasurface are generated by the normally-positioned positive and negative primary sources and these results are presented in Figure 3. The solid and dashed lines in Figure 3 show the magnitude of the average transmission (blue lines), reflection (red lines) and absorption (black lines) coefficients for the controlled and uncontrolled cases respectively. Figure 3(a) shows the behaviour for the positive primary source and Figure 3(b) shows the behaviour for the negative primary source. As noted in Section IV, the proposed active metasurface has been configured to control the wave components with respect to the positive primary source, whilst allowing the incident sound field generated by the negative primary source to propagate unimpeded. It is worth initially highlighting that the performance metrics in the uncontrolled cases for both positive and negative normally-positioned primary sources are identical, demonstrating the conventional reciprocal behaviour prior to control. It is also worth reiterating that the absorption coefficient is non-zero in the uncontrolled case due to the spherical spreading that occurs in the three-dimensional simulated environment. With control, it can be seen from the presented results that the absorption controller achieves near-zero transmission and reflection coefficients with respect to the positive primary source, which leads to near-perfect sound absorption, whilst the performance metrics in the controlled case are equal to the uncontrolled metrics with respect to the negative primary source as shown in Figure 3(b). These results show that the active metasurface achieves nonreciprocal sound absorption when subject to normally-positioned primary sources.

To provide further insight into how the metasurface influences the total sound pressure field, the pressure contour plots in the uncontrolled and controlled cases at 400 Hz are presented in Figure 4. Figure 4(a) shows the uncontrolled incident sound field generated by the normally-positioned positive primary source and Figure 4(b) shows the controlled

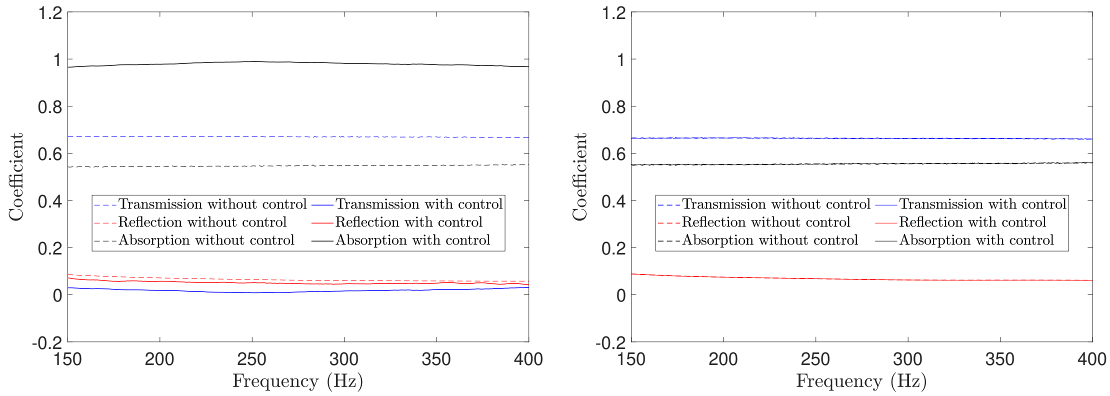

(a) (b)

FIG. 3. The performance of the active metasurface with (solid lines) and without (dashed lines) control in terms of the transmission (blue lines), reflection (red lines) and absorption (black lines) coefficients when the incident waves are produced by the positive (a) and negative (b) primary sources located at the normal.

pressure field. These results show the active metasurface minimises both the transmitted and reflected wave components, leading to near-perfect sound absorption, but the control is clearly limited to within the aperture of the sensor and control source arrays.

B. Obliquely-Positioned Primary Source

In the two-dimensional case considered here, it is also important to investigate the performance of the wave-based actively controlled metasurface when subject to obliquely-positioned positive and negative primary sources. In the case of obliquely-positioned primary sources, the sources have a 45° and -45° angle of incidence respectively, as shown in Figure 1. Similarly to Section V A, the performance metrics for the controlled (solid lines) and uncontrolled (dashed lines) cases have been calculated and these results are presented in Figure 5. Figure 5(a) shows that minimising the transmitted and reflected wave components

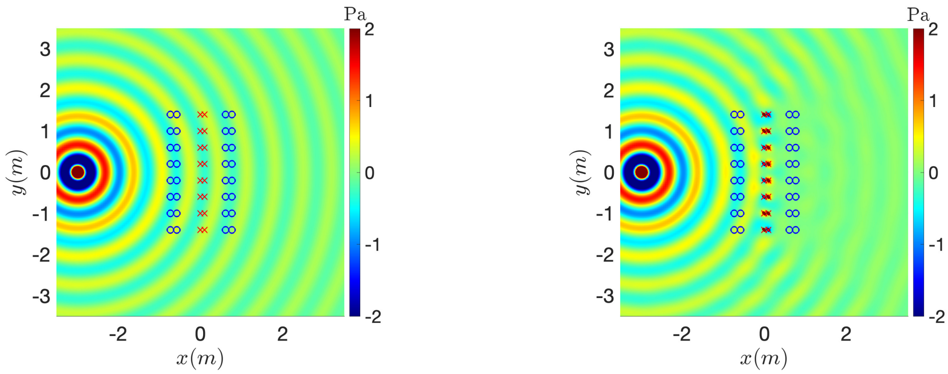

(a) (b)

FIG. 4. The pressure contour plots of the incident sound field corresponding to the pressure generated by the normally-positioned positive primary source without control (a) and with control (b) at 400Hz. The red crosses indicate the monopole control source positions and the blue circles indicate the pressure sensor positions.

maximises the absorption coefficient and it is close to 0.9 across the presented bandwidth. In contrast to the positive primary source case shown in Figure 5(a), the behaviour of the absorption controller with respect to the obliquely-positioned negative primary source shows that the controlled metrics are similar to the uncontrolled case, with some small differences at lower and higher frequencies within the presented bandwidth. These results show that the wave attenuation achieved by the active metasurface in the oblique source case is reduced compared to the normally-positioned case, however, the actively controlled metasurface still achieves significant levels of nonreciprocal sound absorption for the obliquely-positioned primary sources.

As in the case of the normally-positioned primary source, it is insightful to investigate how the active metasurface influences the sound pressure field in more detail and the pressure contour plots are presented in Figure 6. Figure 6(a) shows the incident sound field

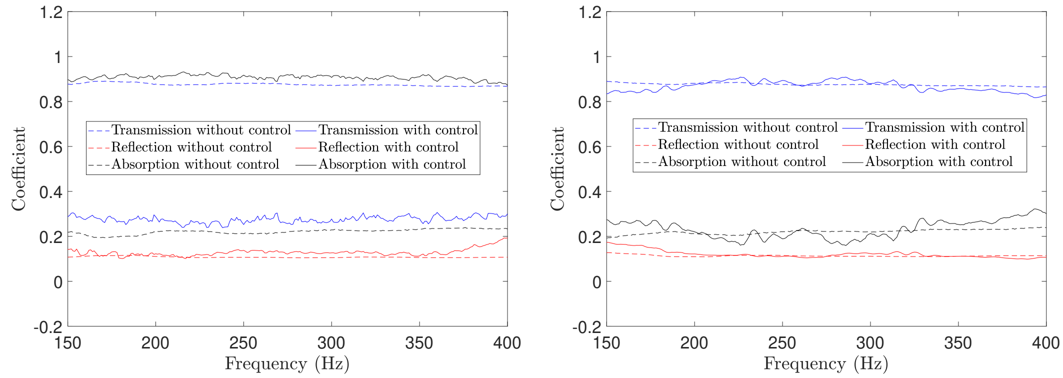

(a) (b)

FIG. 5. The performance of the active metasurface with (solid lines) and without (dashed lines) control in terms of the transmission (blue lines), reflection (red lines) and absorption (black lines) coefficients when the spherical incident waves are produced by the positive (a) and negative (b) primary sources obliquely-positioned.

generated by the obliquely-positioned positive primary source and Figure 6(b) shows the controlled sound field. From these plots it can be seen that the actively controlled metasurface minimises both the transmission and reflection, which leads to the incident wave being absorbed. In the case of the obliquely-positioned primary source, however, it can be seen that diffraction occurs at the edge of the control source array closer to the primary source.

VI. EXPERIMENTAL VALIDATION

The simulation results presented in Section V show that the actively controlled metasurface has the ability to control the various wave components to achieve nonreciprocal sound absorption in a two-dimensional plane. It is important to experimentally validate the simulation results to provide insight into the effects of imperfect free-field conditions, finite-sized sensors and finite-sized loudspeakers, which are used to realise the control sources in a prac-

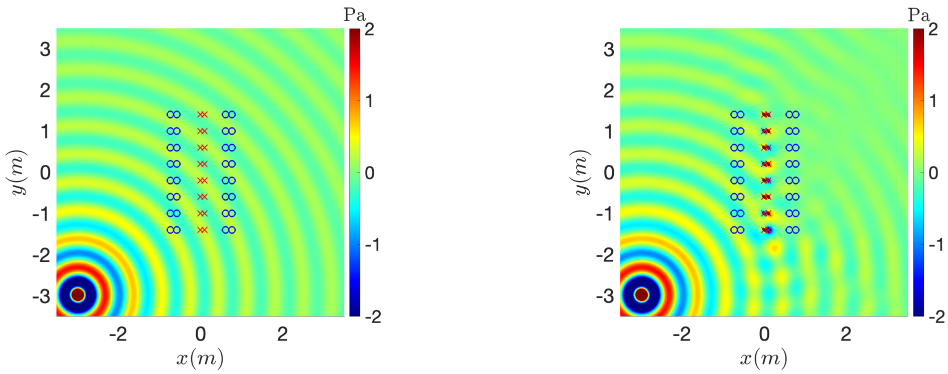

(a) (b)

FIG. 6. The pressure contour plot of the incident sound field correspdonding to the pressure generated by the obliquely-positioned primary source without control (a) and with control (b) at 400Hz. The red crosses indicate the monopole control source positions and the blue circles indicate the pressure sensor positions.

tical system. As mentioned in Section I, the experimental validation has been carried out through offline time-domain simulations using measured responses obtained from a practical system constructed in the anechoic chamber at the ISVR and this system will be described in the following section.

A. Experimental System Description

Figure 7 shows the practical system that has been used to experimentally validate the simulation results presented in Section V. The system shown in Figure 7 has the same physical arrangement and number of sensors and sources as the simulated system shown in Figure 1, with primary sources positioned at normal and oblique angles to the control and sensor arrays, a dual-layer array of control sources located at the centre and two dual-layer arrays of pressure sensors positioned either side of the control sources. The pairs of control sources have been practically realised using two sealed-back Visaton B80 loudspeakers, which have a cone diameter of 8 cm, and share the same enclosure as shown in Figure 7(c). The primary sources have been realised using JBL Control 1 Pro full-range loudspeakers and the microphone arrays have been implemented using 1/4-inch array microphones. All of the data acquisition has been carried out using a Dante-enabled system, which drives each acoustic source individually, via a reconstruction filter and an amplifier, with a logarithmic sine sweep to obtain the impulse responses between each acoustic source and each pressure sensor. The logarithmic sine sweep method has been used because it achieves a higher signal to noise ratio in an anechoic environment and is less time consuming than using white noise to measure the large number of impulse responses[28]. A Larson Davis Cal250 Sound Level Calibrator has been used to calibrate all of the pressure sensors, which are connected via signal conditioning and antialiasing filters to the Analogue to Digital Converters.

B. Results

Having acquired the responses between the primary sources, control sources and arrays of pressure sensors, the performance of the proposed active metasurface and absorption control strategy has been evaluated using offline simulations with the measured responses; this means that the real-time processing requirements have not been considered here, but the physical acoustic effects of the practical implementation have been taken into account. The active metasurface performance has been evaluated, as in the case of the theoretical simulations, for both normally and obliquely-positioned positive and negative primary sources and the results are presented in Figures 8 and 9 respectively. As in Section V, the performance

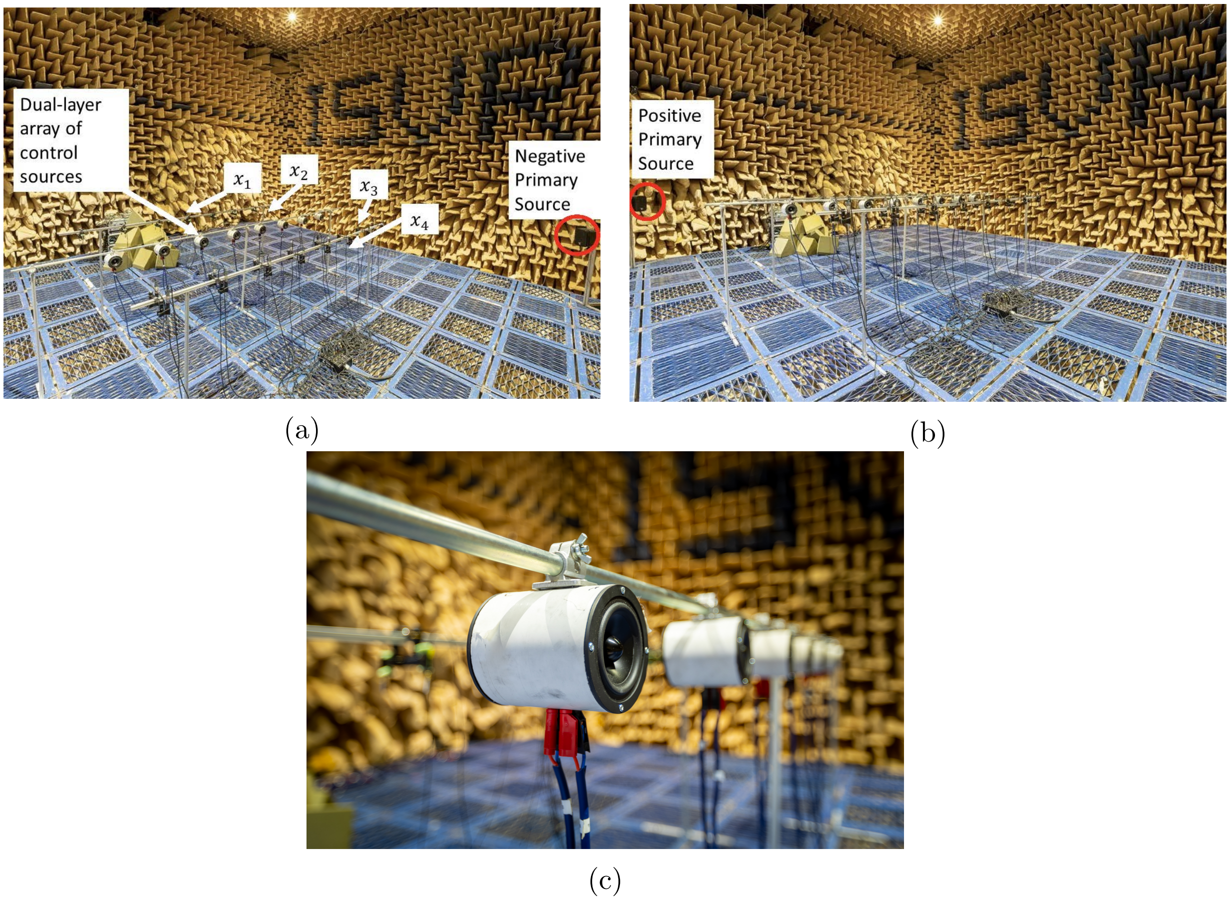

FIG. 7. (a) and (b) show the practical realisation used to obtain the measured response data required to experimentally validate the proposed active metasurface. (c) shows one of the sub-wavelength active unit cells consisting of a pair of sealed back loudspeakers.

metrics before (dashed lines) and after (solid lines) implementing the proposed wave-based active controller have been calculated in each considered case. The experimental results presented in Figures 8 and 9 are largely consistent with the simulation results presented in Section V, confirming the ability of the proposed active metasurface to achieve nonreciprocal sound absorption in a two-dimensional plane. For both the normal and obliquely positioned configurations, the experimental results show greater fluctuations over frequency in the performance metrics compared to the theoretical simulations, which can be related to the presence of the finite-sized sources and sensors introducing scattering into the environment. However, in both cases it is still clear that the positive incident wave is largely absorbed, while the negative incident wave is allowed to pass without significant modification.

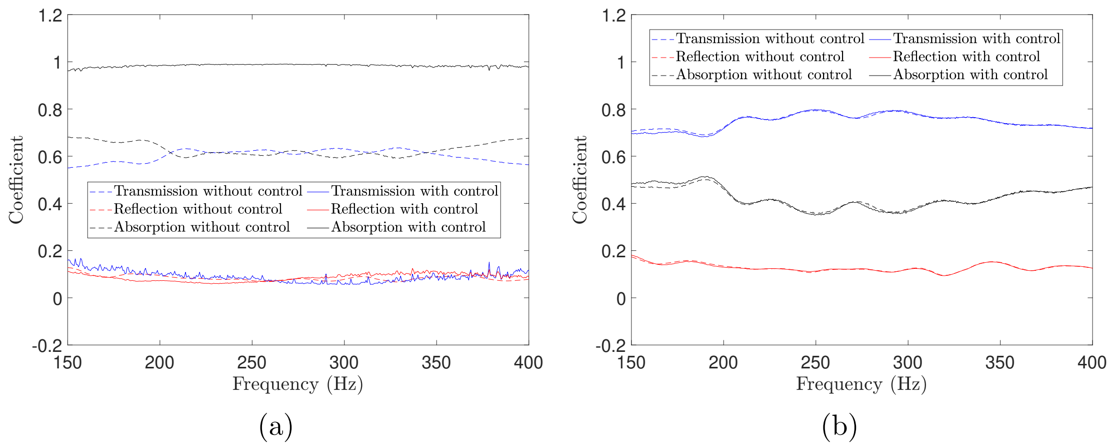

FIG. 8. The performance of the experimental active metasurface with (solid lines) and without (dashed lines) control in terms of the transmission (blue lines), reflection (red lines) and absorption (black lines) coefficients when the incident sound field is generated by the normally-positioned positive (a) and negative (b) primary sources.

VII. CONCLUSIONS

The work presented in this paper has demonstrated through theoretically-modelled and offline experimental simulation-based investigations that the feedforward wave-based active controller and single subwavelength unit cell previously proposed and explored for one-dimensional environments[16] can be extended to a metasurface consisting of a dual-layer array of control sources to control the transmitted and reflected wave components to achieve nonreciprocal sound absorption in a two-dimensional plane within a three-dimensional space.

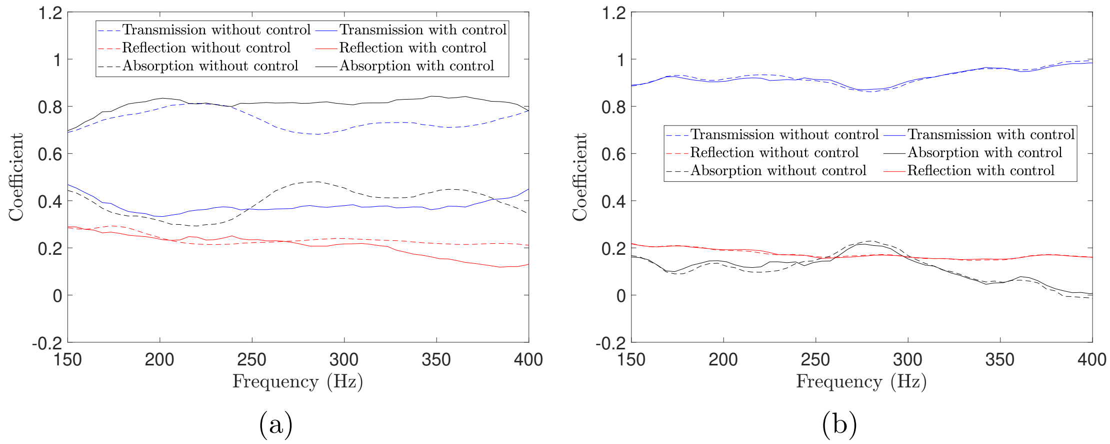

FIG. 9. The performance of the experimental active metasurface with (solid lines) and without (dashed lines) control in terms of the transmission (blue lines), reflection (red lines) and absorption (black lines) coefficients when the incident sound field is generated by the obliquely-positioned positive (a) and negative (b) primary sources.

A wave separation method, which is based on the discrete Spatial Fourier Transform, has been proposed to separate the positive and negative propagating waves in the upstream and downstream of the active metasurface consisting of the array of control sources and arrays of error and reference sensors. A wave-based control strategy for the two-dimensional control problem has then been outlined, which utilises multiple control sources to realise nonreciprocal control over a region of space.

The performance of the wave-based actively controlled metasurface has been evaluated when subject to incident acoustic fields that are generated either by normally or obliquely-positioned positive and negative primary sources. The performance metrics in the controlled and uncontrolled cases have been compared to evaluate the nonreciprocal behaviour of the metasurface. Although the performance of the proposed metasurface is slightly less in the oblique case compared to the normal case, it has been shown that the proposed approach still achieves nonreciprocal sound absorption over the presented bandwidth.

One advantage of the proposed actively controlled metasurface is that it is reconfigurable, such that the direction of the nonreciprocal behaviour can be reversed by changing the reference and error signals used by the controller, which simply requires changing the signals in the control system rather than any physical modifications. In addition to the reconfigurability of the nonreciprocal control approach explored in this paper, it is important for future work to explore how robust the proposed wave-based control strategy is to deviations in the exact positioning of both the sources and sensors forming the active metasurface. Moreover, although in certain situations it would be possible to control multiple incident waves using multiple iterations of the control strategy proposed here, this would not be straightforwardly realisable for the independent control of multiple coherent sources. Therefore, further work is also required to explore the challenges associated with independently controlling multiple incident sources under all circumstances.

ACKNOWLEDGMENTS

This research was partially supported by an EPSRC iCASE studentship (Voucher number: 17000146) and the Intelligent Structures for Low Noise Environments EPSRC Prosperity Partnership (EP/S03661X/1).

AUTHOR DECLARATIONS

Jordan Cheer and Joe Tan have patent WO2023089300A1 and WO2023089301A1 pending.

DATA AVAILABILTY

The data that support the findings of this study are available from the corresponding author upon reasonable request.

REFERENCES

[1]D. N. Zotkin, R. Duraiswami, R. Grassi, and N. A. Gumerov “Fast head-related transfer function measurement via reciprocity,” J. Acoust. Soc. Am. **120**(4), 2202–2215 (2006) doi: 10.1121/1.2207578.

[2]B. S. Kim, G. J. Kim, and T. K. Lee, “The identification of tyre induced vehicle interior noise,” Appl. Acoust **68**(1), 134–156 (2007) doi: 10.1016/j.apacoust.2006.05.020.

[3]B. Liang, S. Guo, J. Tu, D. Zhang, and J. C. Cheng, “An acoustic rectifier,” Nat. Mater **9**(12), 989–992 (2010) doi: 10.1038/nmat2881.

[4]B. I.Popa and S. A. Cummer, “Non-reciprocal and highly nonlinear active acoustic metamaterials,” Nat. Commun **5**, 3398 (2014) doi: 10.1038/ncomms4398.

[5]Z. M.Gu, J. Hu, B. Liang, X. Y. Zou, and J. C. Cheng, “Broadband non-reciprocal transmission of sound with invariant frequency,” Sci. Rep **6**(1), 19824 (2016) doi: 10.1038/srep19824.

[6]A. Baz, "Active nonreciprocal acoustic metamaterials using a switching controller," J. Acoust. Soc. Am. **143**(3), 1376–1384 (2018) doi: 10.1121/1.5026510.

[7]A. Baz, "Active nonreciprocal metamaterial using an eigen-structure assignment control strategy," J. Acoust. Soc. Am. **147**(4), 2656–2669 (2020) doi: 10.1121/10.0001157.

[8]R. Fleury, D. L. Sounas, C. F. Sieck, M. R. Haberman, and A. Alù, "Sound isolation and giant linear nonreciprocity in a compact acoustic circulator," Science **343**(6170), 516–519 (2014) doi: 10.1126/science.1246957.

[9]R. Fleury, D. L. Sounas, and A. Alù, "Subwavelength ultrasonic circulator based on spatiotemporal modulation," Phys. Rev. B **91**(17), 174306 (2015) doi: 10.1103/PhysRevB.91.174306.

[10]Y. Chen, X. Li, H. Nassar, A. N. Norris, C. Daraio, and G. Huang, "Nonreciprocal Wave Propagation in a Continuum-Based Metamaterial with Space-Time Modulated Resonators," Phys. Rev. Appl. **11**(6), 064052 (2019) doi: 10.1103/PhysRevApplied.11.064052.

[11]C. Shen, J. Li, Z. Jia, Y. Xie, and S. A. Cummer, "Nonreciprocal acoustic transmission in cascaded resonators via spatiotemporal modulation," Physical Review B **99**(13), 134306 (2019) doi: 10.1103/PhysRevB.99.134306.

[12]A. Sasmal, N. Geib, B. I. Popa, and K. Grosh, "Broadband nonreciprocal linear acoustics through a non-local active metamaterial," New Journal of Physics **22**(6), 063010 (2020) doi: 10.1088/1367-2630/ab8aad.

[13]N. Geib, A. Sasmal, Z. Wang, Y. Zhai, B. I. Popa, and K. Grosh, "Broadband nonreciprocal linear acoustics through a non-local active metamaterial," Physical Review B **103**(16), 165427 (2021) doi: 10.1103/PhysRevB.103.165427.

[14]Y. T. Fang, and Y. C. Zhang, "Perfect nonreciprocal absorption based on metamaterial slab," Plasmonics **13**(2), 661–667 (2018) doi: 10.1007/s11468-017-0558-5.

[15]Q. Y. Wang, S. Liu, D. Gui, and H. F. Zhang, "Nonreciprocal absorption characteristics of one-dimensional cylindrical magnetized plasma photonic crystals," Physica Scripta **96**(6), 065501 (2021) doi: 10.1088/1402-4896/abede4.

[16]J. Tan, J. Cheer, and S. Daley, "Realisation of nonreciprocal transmission and absorption using wave-based active noise control," JASA Express Letters **2**, 054801 (2022) doi: 10.1121/10.0010454.

[17]J. Fangfang, T. Ye, C. Ying, and L. Xiaojun, "Asymmetric acoustic transmission with a lossy gradient-index metasurface," Applied Physics Letters **113**, 12 (2018) doi: 10.1063/1.5032263.

[18]N. Z. Li, W. Z. Wang, and Y. S. Wang, "Three-dimensional nonreciprocal transmission in a layered nonlinear elastic wave metamaterial," International Journal of Non-Linear Mechanics **125**, 103531 (2020) doi: 10.1016/j.ijnonlinmec.2020.103531.

[19]M. Tamura, "Spatial Fourier transform method of measuring reflection coefficients at oblique incidence. I: Theory and numerical examples," J. Acoust. Soc. Am. **88**, 2259–2264 (1990) doi: 10.1121/1.400068.

[20]M. Tamura, J. F. Allard, and D. Lafarge, “Spatial Fourier-transform method for measuring reflection coefficients at oblique incidence. II. Experimental results,” J. Acoust. Soc. Am. **97**, 2255, (1995) doi: 10.1121/1.412940.

[21]R. Opdam, S. . Hoen, D. De Vries, and M. Voländer “Measurement of angle dependent reflection coefficients with a microphone array and spatial Fourier transform post-processing,” Fortschritte der Akustik, AIA-DAGA **97**, 2255, (205).

[22]S. Wang, H. Sun, J. Pan and X. Qiu, “Near-field error sensing for active directivity control of radiated sound,” J. Acoust. Soc. Am. **144**, 598–607 (2018) doi: 10.1121/1.5049145.

[23]C. Halkyard, and B. Mace, “Feedforward adaptive control of flexural vibration in a beam using wave amplitudes,” Journal of Sound and Vibration **144**, 117–141 (2002) doi: 10.1006/jsvi.2001.4089.

[24]J. Dennis Jr, and R. Schnabel, “Numerical methods for unconstrained optimization and nonlinear equations,” Society for Industrial and Applied Mathematics, (1996).

[25]H. Zhu, R. Rajamani, and K. A. Stelson, “Active control of acoustic reflection, absorption, and transmission using thin panel speakers,” J. Acoust. Soc. Am. **113**(2), 852–870 (2003) doi: 10.1121/1.1534834.

[26]S. J. Elliott, I.M, Stothers, and P.A. Nelson, “A multiple error LMS algorithm and its application to the active control of sound and vibration,” IEEE Transactions on Acoustics, Speech, and Signal Processing **35(10)**, 1423–1434 (1987) doi: 10.1109/TASSP.1987.1165044.

[27]S. J. Elliott, J. Cheer, L. Bhan, C. Shi, and W. S. Gan, “A wavenumber approach to analysing the active control of plane waves with arrays of secondary sources,” Journal of Sound and Vibration **419**, 405–419 (2018) doi: 10.1016/j.jsv.2018.01.028.

[28]G. B. Stan, J. J. Embrechts, and D. Archambeau, “Comparison of different impulse response measurement techniques,” Audio Engineering Society **50**, 249–262 (2002) doi: 10.1016/j.jsv.2018.01.028.